Looking into a 'Blue Hole' – Resolving Magnetization and Structure from the Complex Negative Coompana Anomaly, South Australia

Clive Foss*
CSIRO
Mineral Resources
North Ryde, NSW
clive.foss@csiro.au

Gary Reed
Geological Survey of South Australia
Adelaide, South Australia
gary.reed@sa.gov.au

Tim Keeping
Geological Survey of South Australia
Adelaide, South Australia
tim.keeping@sa.gov.au

Tom Wise
Geological Survey of South Australia
Adelaide, South Australia
tom.wise@sa.gov.au

Rian Dutch
Geological Survey of South Australia
Adelaide, South Australia
rian.dutch@sa.gov.au

SUMMARY

A large (c. 2000nT amplitude, 50 km diameter) negative amplitude TMI anomaly under the Eucla Basin in southwestern South Australia, long known and referred to as the "Coompana Anomaly" has been well resolved by a new high resolution (200 metre line spaced, 80 metre ground clearance) survey flown for the Geological Survey of South Australia. We use parametric inversion to simultaneously derive magnetization direction and spatial distribution of magnetizations giving rise to satellite anomalies both above and around the main anomaly. For the two most prominent satellite anomalies these magnetization estimates agree well with estimates derived from the historic data, but the new survey data provides greater confidence, and reliable mapping of many smaller bodies. The improvement in resolution has allowed us to attempt isolation of the anomaly due to the more voluminous, deeper magnetization, but to date we have not yet been able to recover repeatable results for that deeper magnetization. Magnetization intensity estimates for all investigated anomalies are very high, ranging from about 5 A/m to over 20 A/m (equivalent in intensity to magnetizations from susceptibilities of 0.1 to 0.5 SI). The deeper magnetization is well correlated with a negative gravity anomaly, suggesting that the material generating the main magnetic anomaly has a relatively low density.

Key words: reverse remanent magnetization, magnetic anomaly, South Australia.

INTRODUCTION

The Geological Survey of South Australia (GSSA) has acquired a 256,000 line kilometre airborne magnetic and radiometric survey over part of the Eucla Basin (see Figure 1) previously only covered with 1500 metre line spaced data. The southerly section of the survey area is marked by prominent magnetic anomalies due to reverse remanent magnetization, as shown in Figure 2. The basement geology of this region is substantially obscured by cover and is only poorly known from sparse borehole intersections. Improved mapping of basement lithological units and structures was one of the objectives for collection of the new aeromagnetic data. Preliminary interpretations from this newly acquired magnetic data (Wise et al, 2016) have identified several domains of different basement lithologies, as well as regions covered by volcanic sheets and intruded by magmatic bodies. Integrating the magnetic imagery with existing drillhole constraints suggests that the western part of South Australia had a long-lived, dynamic geological history with major rock-forming events associated with felsic-intermediate magmatism identified in the Coompana Province at c. 1610 Ma, c. 1500 Ma and c. 1180 Ma. Wise et al (2016) estimate an age of between c. 1120 Ma and c. 860 Ma for the intrusive bodies causing the "Coompana Anomaly" and associated satellites.

The Coompana area is at present covered with only sparse gravity data; over the western section of the aeromagnetic infill survey area the gravity station spacing is in excess of 8 km, and over the eastern section it is about 5 km (Figure 3). This coverage is however sufficient to reveal that the main Coompana magnetic anomaly is strongly correlated with a negative gravity anomaly, as shown by coincident regional patterns of the TMI contours and vertical derivative of gravity image in Figure 3. This figure also suggests (although towards the resolution limits of the data) that there may be partial correlation between shallow remanent magnetizations and short-wavelength positive gravity features. If this correlation is borne out by a planned higher resolution gravity survey, then at least some of the shallower reversely magnetised bodies have high densities and are likely to be lithologically different to the main body at depth.

Interpretation of the magnetic field data in this study has initially focussed on estimation of the magnetization direction, as an appropriate magnetization direction is required to determine the spatial distribution of that magnetization. For these predominantly negative anomalies in the Coompana region it is clear that remanent magnetization is dominant, and that it is in a quite different direction to the present geomagnetic field at the site. Estimates of those resultant magnetizations for the four most prominent anomalies in the area are available from the Australian Remanent Anomalies Database (ARAD). An example model description sheet downloaded from the database is also shown in Figure 4, and the statistics for this model are included in Table 1 for comparison with results from this study. The new aeromagnetic data provides superior resolution of these prominent anomalies, upgrades several other anomalies which were detected by the previous survey but insufficiently resolved for reliable analysis, and also reveals numerous additional anomalies undetected in the previous data.

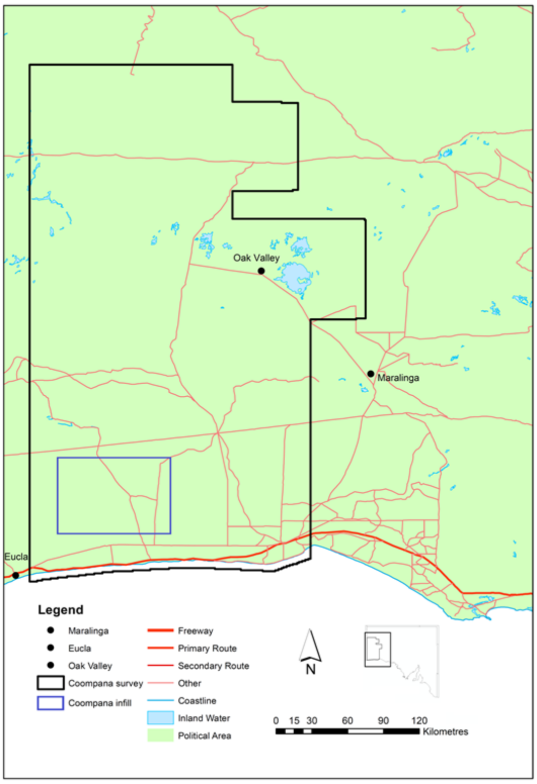

Figure 1 Coompana and infill survey extents

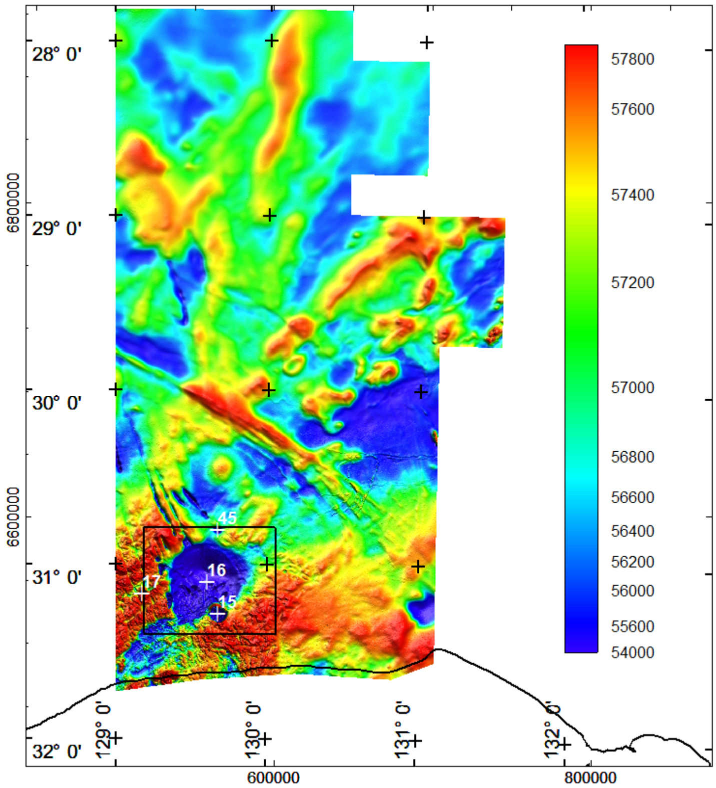

Figure 2 Coompana TMI anomaly

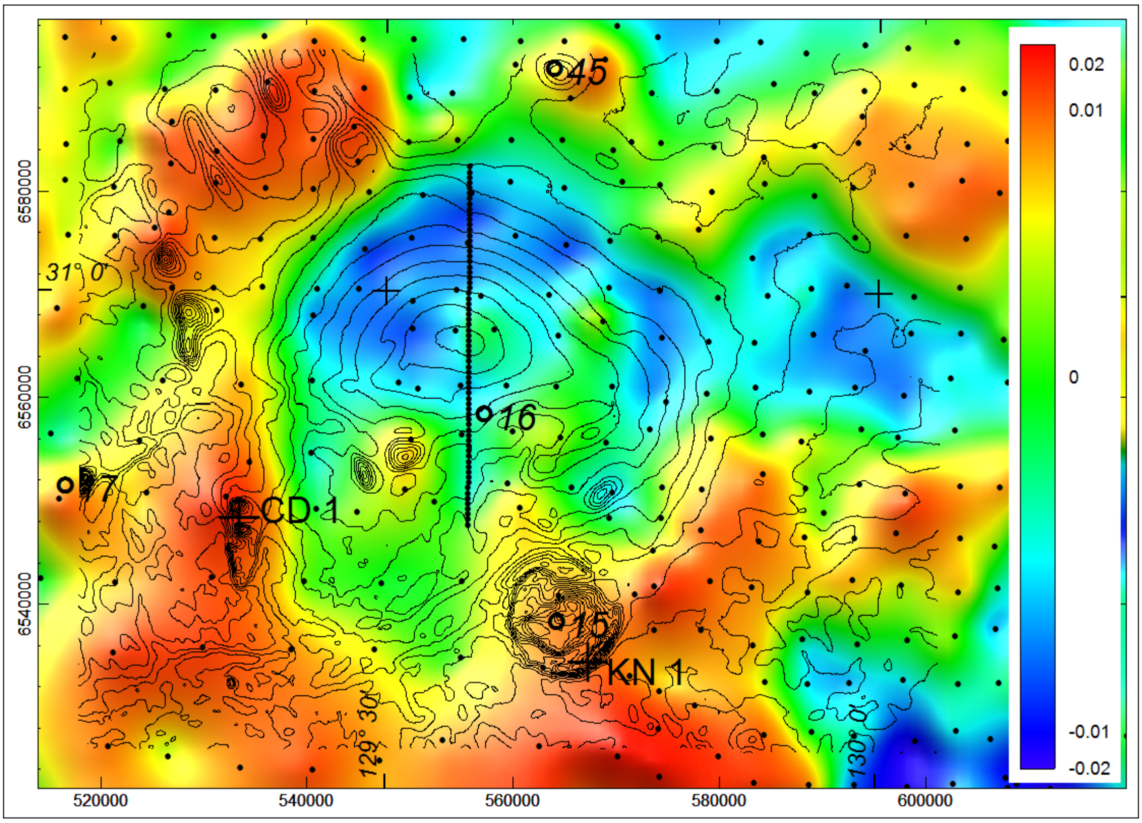

Figure 3 Vertical derivative of 1 km upward continued Bouguer gravity (image), TMI contours, drill holes CD1 and KN1, ARAD anomalies (15, 16, 17 and 45), and gravity stations.

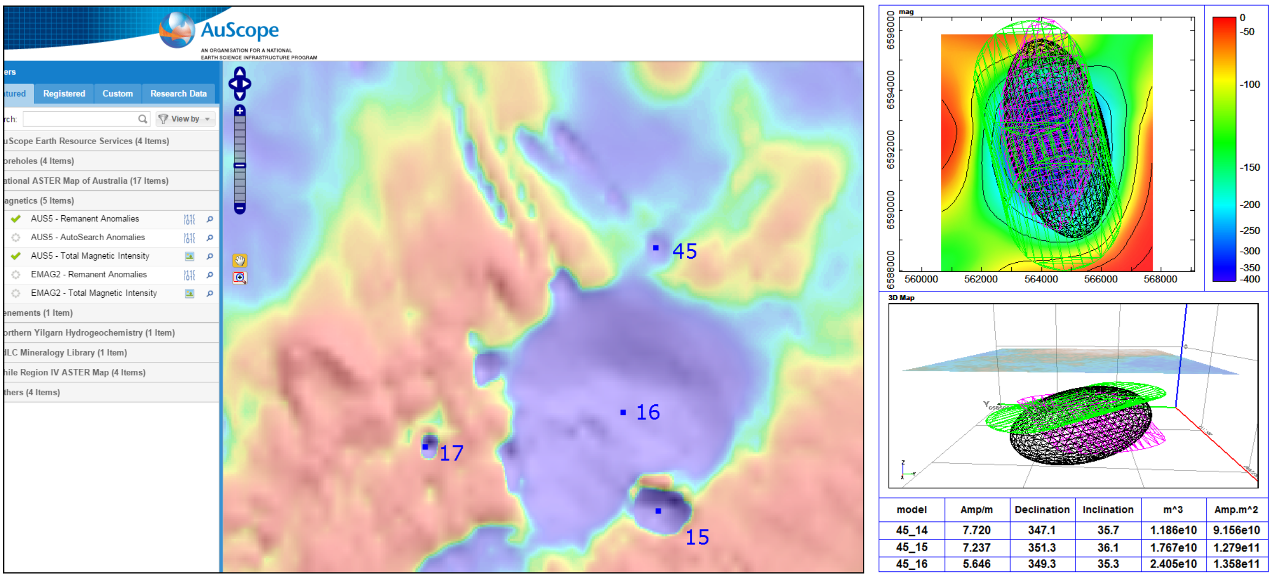

model	Amp/m	Declination	Inclination	m^3	Amp.m^2
45_14	7.720	347.1	35.7	1.186e10	9.156e10
45_15	7.237	351.3	36.1	1.767e10	1.279e11
45_16	5.646	349.3	35.3	2.405e10	1.358e11

Figure 4 (left) ARAD Anomalies in the AuScope Portal, and (right) download of model details for anomaly 45

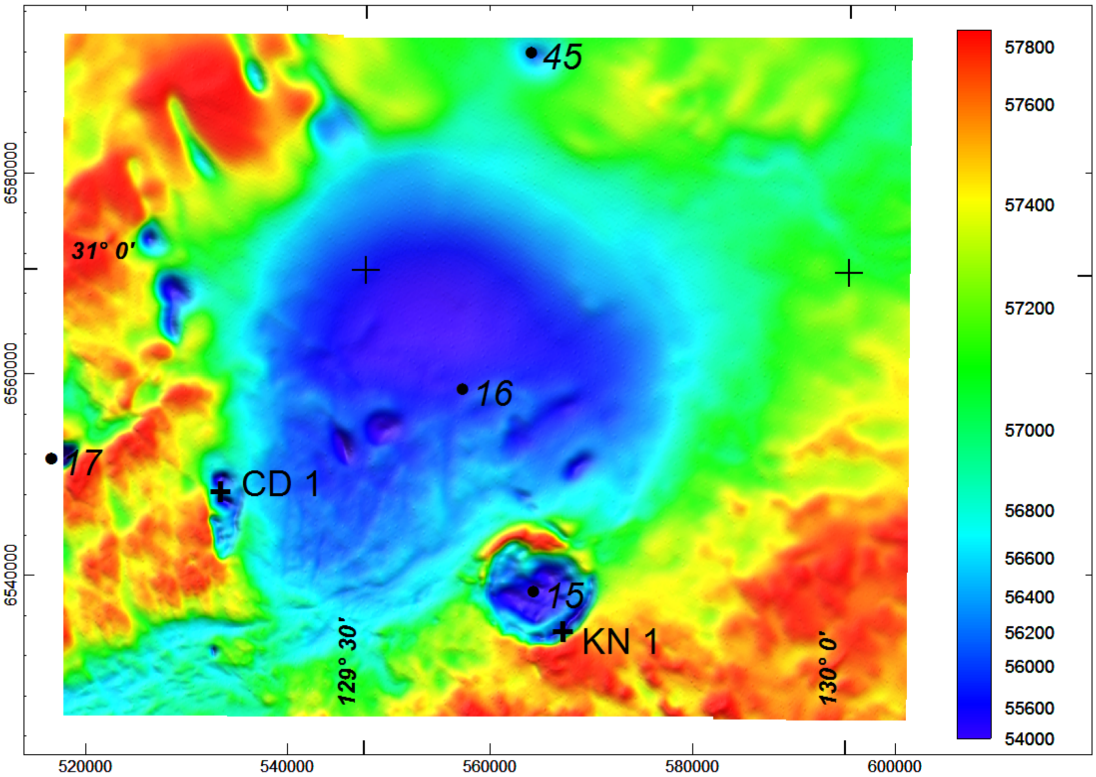

Figure 5 Infill survey TMI image. Boreholes CD1 and KN1 intersected mafic volcanics at 302 and 340 metres respectively

INVERSION METHODOLOGY USED IN THIS STUDY

Clark (2014) provides a comprehensive review of the various methodologies for estimating magnetization direction from magnetic field data. In this study we used the ModelVision Pro^{TM} software package to apply parametric inversion of magnetic field anomalies; a method established by Foss (2004), and subsequently used in studies such as of the Black Hill Norite (Foss and McKenzie, 2011, Pratt et al., 2014) to recover estimates of magnetization direction from magnetic field data. The distribution of studied anomalies is shown over a TMI image derived from the new survey data imaged in Figure 5. The new survey has resolved considerable additional detail in the magnetic field, with several satellite anomalies poorly resolved in the previous coverage now amenable to detailed analysis. For compact, simple anomalies we mostly used flat-topped cylinders of elliptic cross-section. For larger and more complex sources we performed an initial inversion using elliptic cylinders, but then transformed those bodies to more general plunging prisms of polygonal cross-section. Magnetization is a bulk property of a magnetization model, and after an approximate initial fit to the anomaly, the magnetization direction remains quite consistent as the later stages of inversion resolve the finer details of body shape.

The anomalies we have investigated to date include three of the four anomalies in ARAD (anomalies 16, 17 and 45). The fourth anomaly (anomaly 15) is shown by the present survey data to be a complex body with to at least two zones with different magnetization directions. This degree of complexity was not resolved by the previous survey data, for which the anomaly was interpreted as due to a single, homogeneous magnetization.

Figure 6 shows the inversion results for ARAD anomaly 45, resampled by the new survey data. Multiple east-west flight-lines at a spacing of 400 metres have been inverted. The background field was interpreted and represented with a 2nd order polynomial surface. An elliptic pipe was introduced beneath the anomaly and given a steep reverse remanent magnetization to produce an approximate match to the measured anomaly, and the spatial and magnetization parameters of the model were simultaneously inverted to find the rms best-fit model of that geometry. Figure 6 shows the model and the data fit of the model-computed field at completion of inversion. The top of the pipe has a depth below surface of approximately 1500 metres and a steep plunge to the north. The best-estimated magnetization direction of inclination +34°, declination 342°(line 8 in table 1) is only 6° different to the mean direction reported in ARAD for 3 inversions of the historic data using several different model geometries (lines 5 to 7 in table 1). To investigate the stability of the inversion process we interpolated total gradient of TMI data onto the flight lines, and separately inverted that data for magnetization intensity and spatial parameters (not magnetization direction) of two elliptic pipe models, one assigned an induced direction magnetization, and the other a magnetization in the direction best-estimated from inversion of the TMI data. The total gradient data is only weakly sensitive to magnetization direction, and those two inversions produced similar results (shown in Figure 7), approximately coincident with the magnetization mapped by the TMI inversion. This result confirms that the distribution of magnetization can be approximately recovered from total gradient data regardless of the assumed magnetization direction. Subsequently we inverted those two models against the TMI data for magnetization direction only. If the models approximately map the spatial distribution of magnetization, then they should also yield approximately correct estimates of the direction of that magnetization. TMI inversion of the model initially generated using an induced magnetization direction yielded a magnetization direction within 11°of the best-estimate. TMI inversion of the magnetization direction of the model initially generated by total gradient inversion using the best-estimated magnetization direction, recovered that direction within 6°. These results are consistent with test inversions of synthetic data, which show a marginally superior performance of simultaneous inversion of spatial and magnetization parameters over this staged process of inverting first for distribution (with total gradient data), and then separately for magnetization direction (with TMI data). Table 1 reports inversion results for downloaded models for ARAD anomalies 16, 17 and 45, and these magnetization directions are also plotted in Figure 10. Inversion of the new survey data defining the relatively simple ARAD anomaly 17 also produces similar results to inversion of the historic data, with a difference of less than 6° between two inversions of the new data using different geometry models (elliptical and polygonal pipes), and less than 11° between the mean of those directions and the mean direction from two ARAD inversion models. The difference between magnetization directions recovered in this study for ARAD anomalies 17 and 45 is 24°, which is significant. This is a difference primarily in inclination, which can be explained either as an intrinsic difference in remanent magnetization direction for the two bodies (for instance due to apparent polar wander between different emplacement ages), or as a change in Koenigsberger ratio between remanent and induced magnetizations, which causes the resultant magnetization directions to smear out along a great circle joining the remanent and geomagnetic field directions.

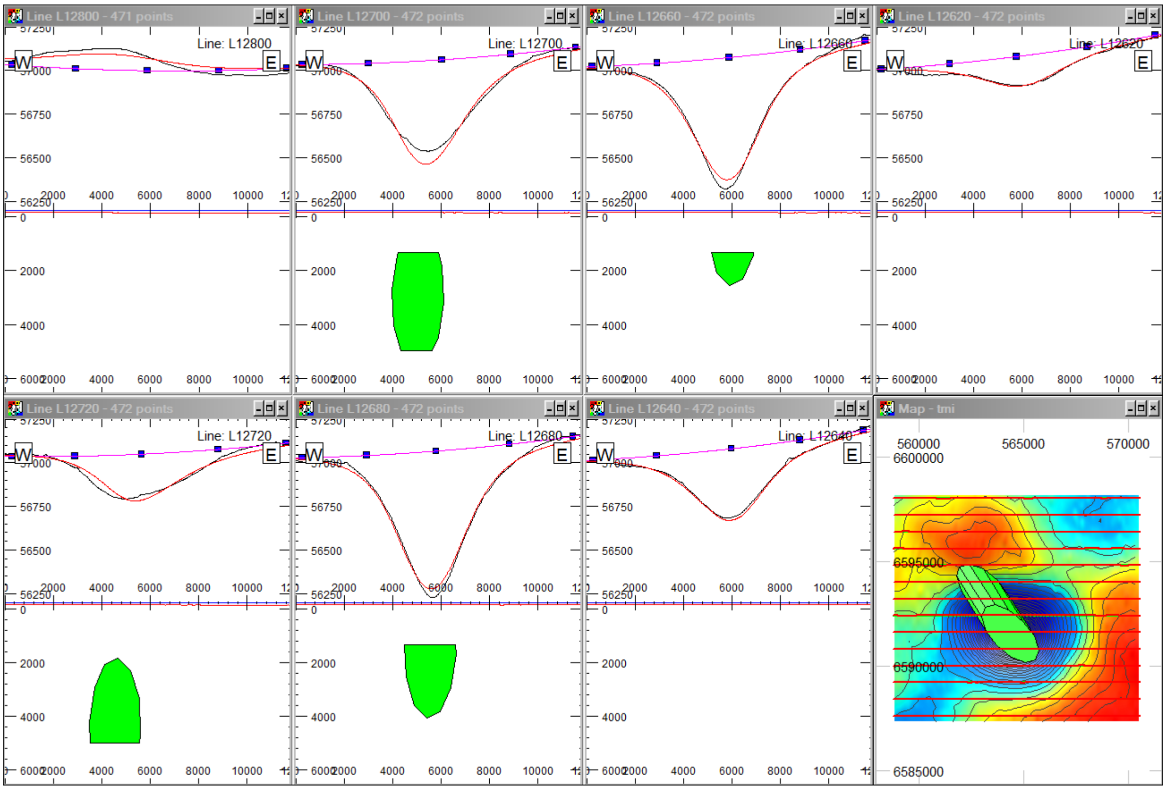

Figure 6 Model sections inverted to match TMI along new flight lines over ARAD anomaly 45 (the data curve is black, the assumed background curve is purple, and the model computed curve is red)

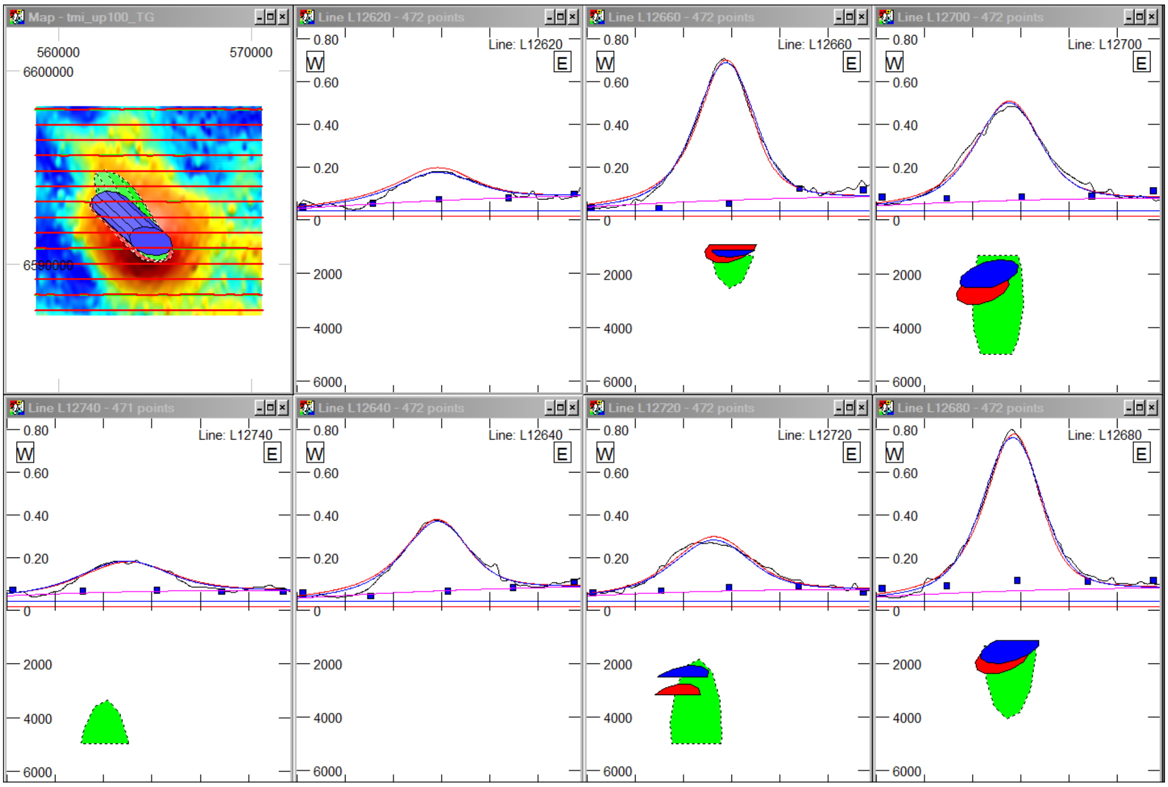

Figure 7 Model sections inverted to match total gradient of TMI along new flight lines over ARAD anomaly 45. The red inversion body has an induced magnetization; the blue inversion body has the estimated remanent magnetization; the green TMI inversion body is shown for comparison

Inversion of the main Coompana anomaly is more problematic. From the historic data it was evident that this anomaly has superimposed field variations due to shallower magnetizations, particularly across its southern half. These superimposed magnetizations are now far better resolved by the new survey data, supporting postulated (but still interpretive) separations to isolate the major anomaly itself. In order to investigate repeatability of this process, we inverted data on north-south tie lines across the anomaly at 2 km spacing, and separately a dataset composed of every tenth east-west flight line across the anomaly, also at 2 km spacing. Illustration of the inversion of the flight-line data is shown in Figure 8. The top right-hand map shows the measured TMI, including superimposed anomalies from shallower magnetizations. The selection of data for inversion of the main anomaly is shown in the top left-hand image. The grid image of the model-computed field at completion of the inversion shown in the bottom left-hand image matches the main features of the isolated TMI data, but not all of the subtle gradient variations, suggesting that the model may provide an overestimation of the depth of the magnetization. The lower right-hand map in Figure 8 shows the top plan of both the flight-line and tie-line models, which are broadly consistent. The models also show considerable overlap in the perspective view of Figure 9. However, there are sufficient differences between those models, which we interpret to arise from problematic separation from the regional background field and from the extensive overlapping anomalies, to give rise to differences in the magnetization directions they provide. The difference in estimated magnetization directions between the flight-line and tie-line inversion results, listed in Table 1 and plotted in Figure 10 is 43°, and the differences between both those directions and the shallower inclination estimate from the corresponding ARAD inversion of the historic data are 44°and 42° respectively. We conclude that none of these current estimates is reliable, and are attempting to improve isolation of the main anomaly, as we are keen to compare its direction of magnetization with estimates from a similar pattern anomaly under the Nullarbor to the east, and also with magnetization directions recovered from deep magnetizations beneath the Officer Basin to the northwest. The depths to the tops of the two models are 7.6 km and 8.4 km for the flight-line and tie-line inversions respectively, although close comparison of the local changes in gradient of the measured and model-computed fields suggests that some of the magnetization may be somewhat shallower than this.

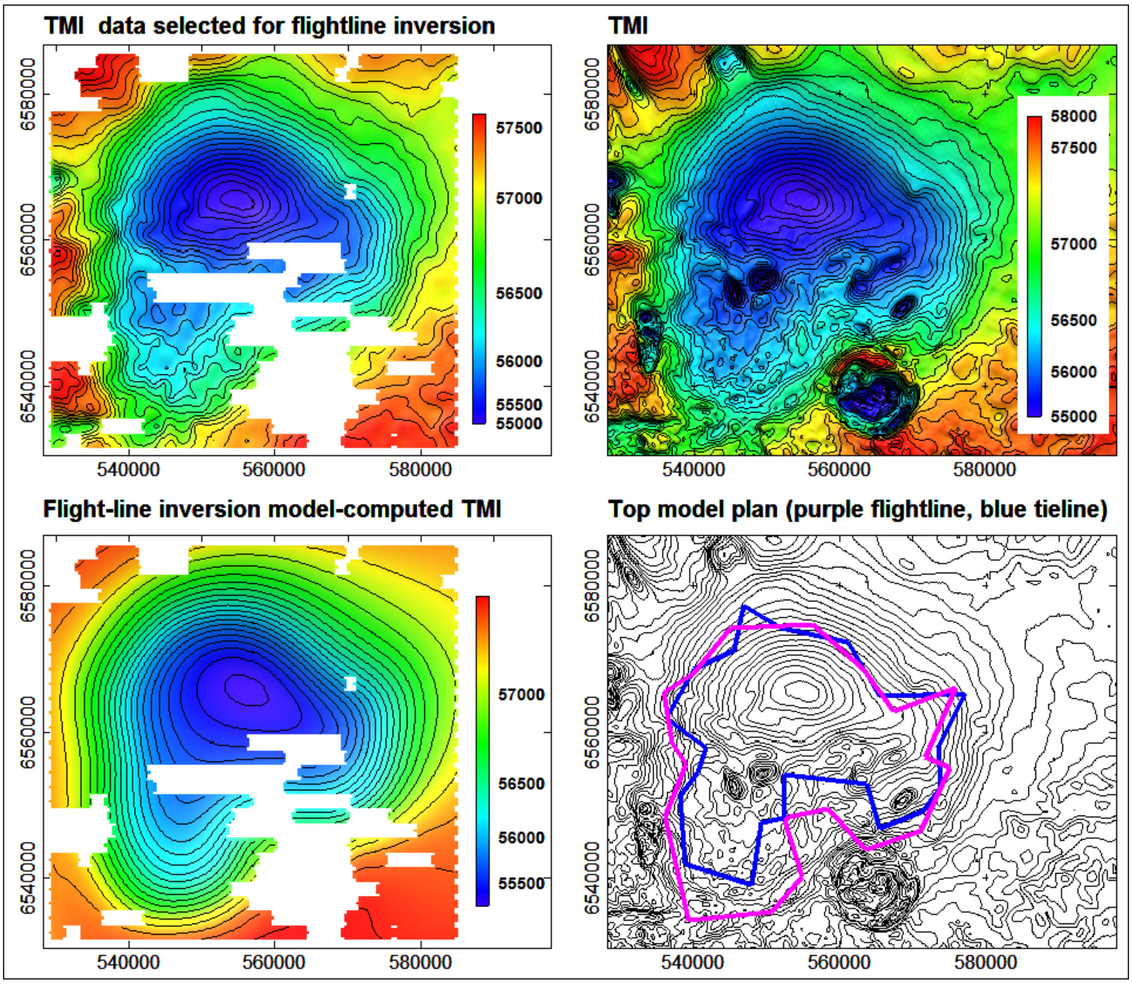

Figure 8 (top right) TMI; (top left) TMI selected for flight-line inversion; (bottom left) model-computed TMI; (bottom right) plan of model top faces with TMI contours

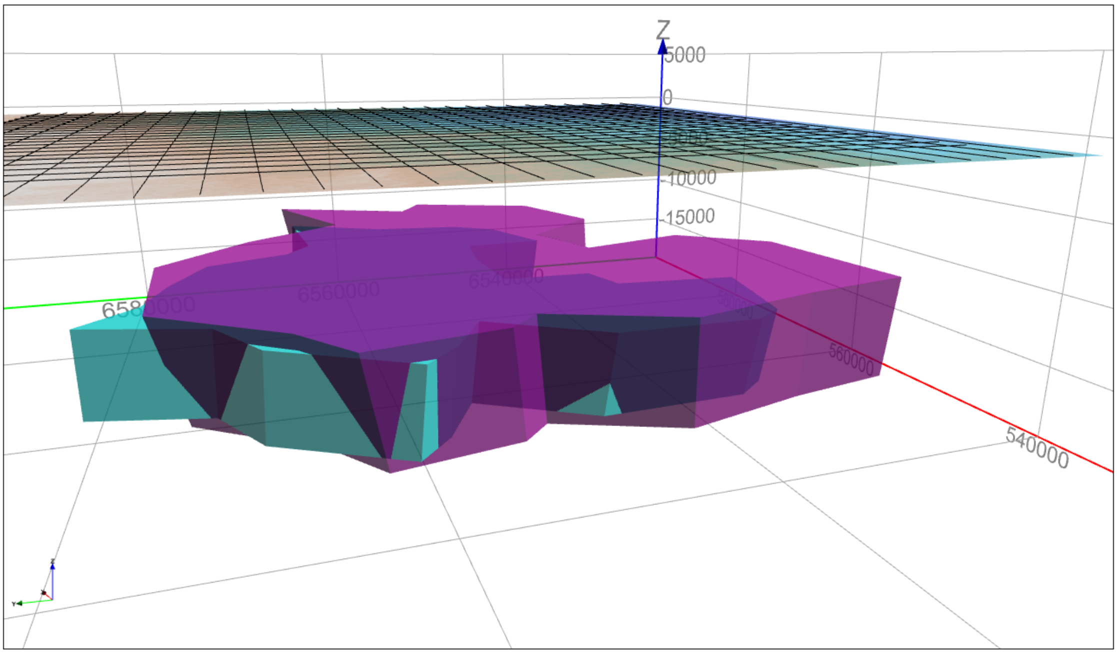

Figure 9 Perspective view of the models from inversion of the flight line data (purple) and the tie line data (turquoise)

	ARAD anomaly	ARAD model	Body type	Description	Inclination	Declination	Intensity A/m	Volume m3	Moment A.m2
1	17	12	Elliptic pipe		+50.4	331.8	16.87	5.26E9	8.87E10
2	17	13	Polygonal prism		+51.0	336.6	19.67	3.99E9	6.65E10
3	17	This study	Elliptic pipe		+59.9	342.0	20.38	6.23E9	1.27E11
4	17	This study	Plunging prism		+56.1	349.9	24.84	4.73E9	1.17E11
5	45	14	Circular pipe		+35.7	347.1	7.72	1.19E10	9.16E10
6	45	15	Elliptic pipe		+36.1	351.3	7.24	1.77E10	1.28E11
7	45	16	Ellipsoid		+35.3	349.3	5.65	2.41E10	1.36E11
8	45	This study	Elliptic pipe	TMI inversion	+34.2	342.1	10.42	1.647E10	1.72E11
9	45	This study	Elliptic pipe	TG (induced) then TMI inversion	+45.1	342.8	18.02	4.54E9	8.18E10
10	45	This study	Elliptic pipe	TG (remanent) then TMI inversion	+38.7	337.4	22.21	3.38E9	7.51E10
11	16	11	Polygonal prism		+36.8	265.3	32.95	4.75E12	1.57E14
12	16	This study	Polygonal prism	TMI flight-line inversion (27 lines, 2 km spacing)	+75.6	220.1	11.61	7.42E12	8.61E13
13	16	This study	Polygonal prism	TMI tie-line inversion (23 lines, 2 km spacing)	+68.2	317.6	16.43	3.850E12	6.33E13

Table 1 Statistics of magnetizations for 3 corresponding anomalies downloaded from ARAD and derived in the present study

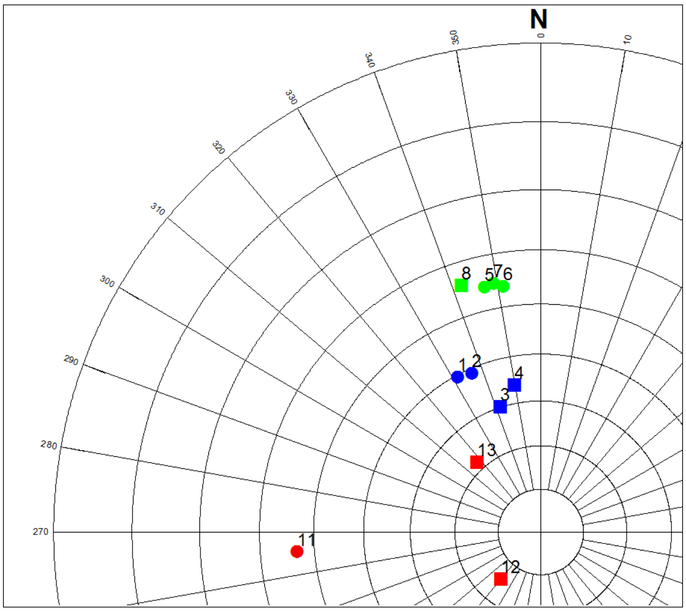

Figure 10 Stereonet of inversion magnetization estimates (blue ARAD anomaly 17, red ARAD anomaly 16, green ARAD anomaly 45; circles downloaded from ARAD, squares derived in this study)

CONCLUSIONS

The new Coompana aeromagnetic survey has mapped the magnetic field of the region in unprecedented resolution. This has improved confidence in interpretation of anomalies mapped by the historic data coverage, and has resolved many smaller anomalies of interest. We have established that for discrete, compact sources we can recover magnetization direction by parametric inversion of their individual anomalies. Estimation of these magnetization directions allows reliable positioning of the magnetizations, and this will be input into drilling programs currently being planned. Investigating the main anomaly, which is partially covered by shallower magnetizations, is more problematic and we have not as yet recovered a reliable magnetization direction for this anomaly. The intensities of magnetization for sources of the different anomalies range between 5 and 20 A/m, which is high; equivalent to magnetizations arising from susceptibilities of between 0.1 and 0.5 SI. The main anomaly is due to magnetizations substantially at depths in excess of 7 km, and has a strong correlation with a negative gravity anomaly, suggesting that it is a relatively low density body.

REFERENCES

Foss, C.A., 2006, Evaluation of strategies to manage remanent magnetization effects in magnetic field inversion: SEG Technical Program Expanded Abstracts 2006: pp. 938-942.

Foss, C.A., and McKenzie, K.B., 2011, Inversion of anomalies due to remanent magnetization: an example from the Black Hill Norite of South Australia: Australian Jurnal of Earth Sciences, 58, 391-405.

Pratt, D. A., McKenzie, K.B., and White, A.S., 2014, Remote remanence estimation (RRE): Exploration Geophysics, 45, 314-323.

Wise, T.W., Pawley, M.J., and Dutch, R.A. 2016, Preliminary interpretations from the 2015 Coompana aeromagnetic survey, MESA Journal, v. 79, p. 24-31.